Research Paper

Characterization of gas hydrate morphology from seismic data in the northern South China Sea

Danqing Dai, Xuewei Liu*, Zaiming Zhang

School of Geophysics and Information Technology, China University of Geosciences (Beijing), Beijing, 100083, China

ABSTRACT

The second gas hydrate expedition drilled 13 sites in northern South China Sea and recovered a large amount of gas hydrate. The logging data and core analysis indicate that the gas hydrate occurs as solid nodules, disseminated within pore spaces of sediments and fracture fillings in veins. In this study, we examine two sites (sites 08 and 16), where gas hydrates occur both near the BSR and near the surface. We use the mesoscopic-loss mechanism to study the reflection coefficient versus frequency at BSR in seismic frequency band. When the seismic wave passes through the pore-filling gas hydrate sediments, the high frequency energy is much reduced and the low frequency energy of reflected waves at BSR is strong. When the seismic wave passes through the fracture-filling gas hydrate sediments, the high frequency wave is easily propagated and its reflected energy at BSR is strong. This difference of these at BSR between two types of gas hydrate contained sediments can be utilized to distinguish the gas hydrate morphology. The seismic data in northern South China Sea is analyzed and the results correspond well with the forward modeling approach.

© 2018, China University of Geosciences (Beijing) and Peking University. Production and hosting by Elsevier B.V. This is an open access article under the CC BY-NC-ND license (http://creativecommons.org/licenses/by-nc-nd/4.0/).

1. Introduction

Gas hydrates are formed due to the high hydraulic pressure present under the cold seabed over long periods of time. Gas hydrates are stable under the temperature and pressure conditions typical of water depths greater than 500 m in oceanic sediments along the continental margins. In the South China Sea, gas hydrates were found by the Guangzhou Marine Geologic Survey (GMGS) in 2007 (Zhang et al., 2007).

Gas hydrates can be summarized as pore-filling or fracture-filling based on their morphologies in sediments. In the process of exploiting hydrates, the gas hydrates existence in sediments must first be known. The exploitation methods would be different according to the hydrate morphology. In 2013, GMMS once again conducted a drilling program that targeted the gas hydrate deposits in the northern South China Sea. A total of 23 holes were drilled at 13 sites (Zhang et al., 2014b). The logging data and core analysis indicated the occurrence of gas hydrates from approximately 5 m to 220 m below mudline (BML). Gas hydrates occur as solid nodules,

disseminated within pore spaces of sediments and fracture fillings in veins (Yang et al., 2014; Zhang et al., 2014a, b).

Nowadays, many researchers have studied the presence and amounts of gas hydrate. Still, we cannot identify the morphology of gas hydrate in sediments before we drill the site. There's no such research to give a way to solve the problem. In this paper, we will discuss how to identify the gas hydrate morphology in sediments based on the frequency dependent reflection coefficient.

2. Mesoscopic-loss mechanism

Previous studies found that the major cause of attenuation occurs at three scales: macroscopic, mesoscopic, and microscopic. At macroscopic scale, the Biot theory (Biot, 1962) gives the attenuation mechanisms. The drawback of this is that the macroscopic-flow mechanism underestimates the velocity dispersion and attenuation in rocks. At the microscopic scale, the so-called squirt flow is incapable of describing the measured levels of dissipation at seismic frequencies. Pride et al. (2004) studied the mesoscopic loss mechanism and found that the mesoscopic model provides the proper attenuation to explain the field data, and therefore, we use the mesoscopic theory to study the reflection coefficient varying with frequency at BSR.

* Corresponding author.
E-mail address: liuxw@cugb.edu.cn (X. Liu).
Peer-review under responsibility of China University of Geosciences (Beijing).

2.1. Patchy saturation model

White et al. (1975) were the first to introduce the mesoscopic-loss mechanism. They considered gas pockets in a water-saturated porous medium and porous layers alternately saturated with water and gas, respectively.

For simplicity, we consider two porous media with thicknesses d_1 and d_2. Here, d_1 and d_2 are much smaller than the seismic wavelength. These two media are layered periodically with the period of $(d_1 + d_2)$. Based on White's model, Carcione and Picotti (2006) presented the formula for the complex modulus for a P-wave traveling perpendicular to the thinly layered stratification. It is given by

$$E = \left[\frac{1}{E_0} + \frac{2(r_2 - r_1)^2}{i\omega(d_1 + d_2)(I_1 + I_2)}\right]^{-1} \tag{1}$$

$$E_0 = \left(\frac{p_1}{H_1} + \frac{p_2}{H_2}\right)^{-1} \tag{2}$$

where $p_S = d_s/(d_1 + d_2)$ with $s = 1, 2$ representing medias 1 and 2. Omitting the subscript s, we have for each medium

$$r = \frac{BM}{H} \tag{3}$$

which is the ratio of fast P-wave fluid tension to total normal stress,

$$I = \frac{\eta}{k\kappa}\coth\left(\frac{kd}{2}\right) \tag{4}$$

which is an impedance related to the slow P-wave, where k is the complex wave number of the slow P-wave velocity and is given by

$$k = \sqrt{\frac{i\omega\eta H}{\kappa M\left(K_{dry} + \frac{4}{3}\mu_{dry}\right)}} \tag{5}$$

M, C and H are elastic moduli calculated from the following expression:

$$M = \frac{K_g}{1 - \frac{K_{dry}}{K_g} + \phi\left(\frac{K_g}{K_f} - 1\right)} \tag{6}$$

$$H = K_{dry} + \frac{4}{3}\mu_{dry} + BC, \text{ and } C = BM \tag{7}$$

where K_g, K_f, and K_{dry} are the bulk moduli of the mineral grain, the pore fluid, and the drained rock frame, respectively; and $B = 1 - K_{dry}/K_g$, which is called Biot's coefficient.

The P-wave velocity V_P and S-wave velocity V_S of the periodic stratification are given by

$$V_P = \left[\text{Re}\frac{1}{V}\right]^{-1} \tag{8}$$

$$V_S = \sqrt{\frac{\mu_{dry}}{p_1\rho_{b1} + p_2\rho_{b2}}} \tag{9}$$

where $\text{Re}(V)$ represents the real and imaginary parts of the complex velocity V, which is expressed as

$$V = \sqrt{\frac{E}{p_1\rho_{b1} + p_2\rho_{b2}}} \tag{10}$$

where ρ_{b1} and ρ_{b2} are the bulk densities of medias 1 and 2.

2.2. Double-porosity model

Pride and Berryman (2003a, b) studied P-wave dispersion and attenuation created by lithological variations. The double-porosity is modeled as a mixture of two porous phases saturated by a single fluid. When elastic waves at different frequencies squeeze the rock matrix, pressure differences will appear inside the pore fluid as a result of two different kinds of pore structures. That leads to fluid flow from high pressure region with more compliant portions to the low pressure region with stiffer portions. Energy loss occurs in the process.

In the model, P-wave velocity V_P and S-wave velocity V_S are expressed below:

$$V_P = 1/\text{Re}\{s\} \tag{11}$$

$$V_S = \sqrt{G/\rho} \tag{12}$$

s is the slowness of Biot theory.

$$s^2 = b + \sqrt{b^2 - \frac{\rho\tilde{\rho} - \rho_f^2}{MH - C^2}} \tag{13}$$

$$b = \frac{\rho M + \tilde{\rho}H - 2\rho_f C}{2(MH - C^2)} \tag{14}$$

where H, C and M are the Biot (1962) poroelastic moduli defined as

$$H = K_U + 4G/3 \tag{15}$$

$$C = BK_U \tag{16}$$

$$M = \frac{B^2}{1 - K_D/K_U}K_U \tag{17}$$

The complex inertia $\tilde{\rho}$ corresponds to rewriting the relative flow resistance as an effective inertial effect

$$\tilde{\rho} = -\eta/[i\omega k(\omega)] \tag{18}$$

where $1/k = v_1/k_1 + v_2/k_2$, K_D is the effective drained bulk modulus of the double-porosity composite, K_U is the effective undrained bulk modulus, G is the shear modulus of the composite. We do not consider the S-wave dispersion here. The detail introduction can be found in the Appendix.

3. The frequency dependent reflection coefficient at BSR of pore-filling gas hydrate layer

We built a model to study the reflection coefficient at BSR. The model consists of two layers. When gas hydrate fills in the pore space of layers, the upper layer contains gas hydrate and water in the pore. The layer below the gas hydrate sediment is alternately saturated with water and gas. The rock matrix of the two layers is the same, and consists of several minerals showed in the table below. As mentioned in the above introduction, if the rock has mixed saturation, the seismic dispersion will be high according to White's model. In this case, we use the patchy saturation model to study the two layers.

In the model, all the parameters take the Dongsha area as the reference (Table 1). In the upper layer, the porosity is $\phi_1 = 0.5$, the initial permeability is $k_0 = 0.5$ mD, the gas hydrate filled permeability is $k_1 = k_0(1 - S_h)^{7.9718}$ (Li et al., 2014), the saturation of gas hydrate is $S_h = 0.15$ (Wang et al., 2009). In the lower layer, the porosity is $\phi_2 = 0.55$, the permeability is $k_2 = 10$ mD.

In order to discuss the reflection coefficient versus frequency (RVF), we use the Zoeppritz equation. In the equation, the dispersion is considered, that is to say the P-wave velocity varies with frequency. Correspondingly, the frequency dependent reflection coefficient can be derived. We only consider the P-wave dispersion and assume the shear wave doesn't have dispersion. We further calculate the ratio of reflection coefficient to get the relative change. When $f_0 = 1$ Hz, the reflection coefficient should be $R(f_0)$, the ratio of reflection coefficient can be expressed as $ratio = \frac{R(f) - R(f_0)}{R(f_0)} \times 100\%$, and then we can get the following curves.

The reflection coefficient represents the ratio of reflected wave energy and incident wave energy. When gas exists beneath the

Table 1
The rock physics parameters of model.

	Bulk modulus (GPa)	Shear modulus (GPa)	Density (g/cm³)	Volume fraction
Quartz	36.6	45	2.65	0.3
Muscovite	61.5	41.1	2.79	0.2
Plagioclase	75.6	25.6	2.63	0.08
Clay	20.9	6.85	2.58	0.22
Calcite	76.8	32	2.71	0.2
Water	2.5	0	1.032	–
Pure hydrate	5.6	2.4	0.92	–

pore-filling gas hydrate sediment, the reflection coefficient at BSR is negative (Fig. 1). With the increase of frequency, the absolute value of reflection coefficient decreases. That is to say, the energy of low frequency reflected wave is strong and the energy of high frequency reflected wave is weak. This trend doesn't change with different incident angles.

From Fig. 2 we can see, with the increasing saturation of gas hydrate, the absolute value of reflection coefficient increases. The absolute value of reflection coefficient decreases with frequency and this RVF trend is more prominent at low saturation of gas hydrate.

4. The frequency dependent reflection coefficient at BSR of fracture-filling gas hydrate layer

We built a model to study the reflection coefficient at BSR. The model consists of two layers. When gas hydrate fills in the fracture of rocks, the upper layer contains gas hydrate. In this case, the P-wave dispersion will be created by lithological variations. As we introduced above, the double-porosity theory could describe such effects. We use the double-porosity theory to model the gas hydrate layer. The upper layer consists of two solid phases. The host phase which forms the rock matrix is comprised of several minerals (Table 1). The other is the gas hydrate solid phase. Water fills in pores. The layer below the gas hydrate sediment is patchy saturation model with two porous media, which is alternately saturated with water and gas.

In the upper layer, the porosity is $\phi_1 = 0.5$, the initial permeability is $k_0 = 0.5$ mD, the gas hydrate filled permeability is $k_1 = k_0(1 - S_h)^{7.9718}$ (Li et al., 2014), the saturation of gas hydrate
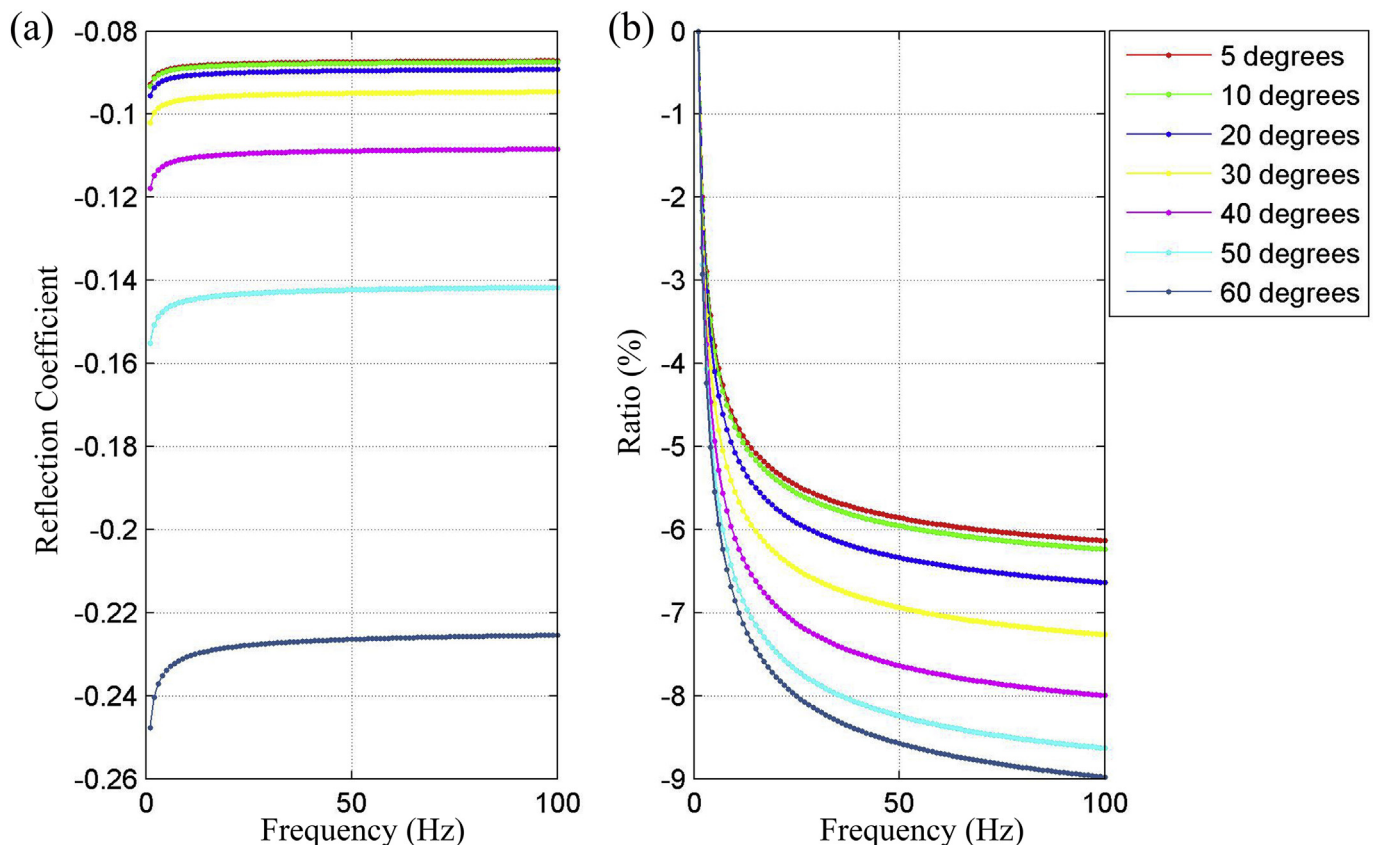

Figure 1. (a) The absolute change of reflection coefficient versus frequency with different incident angles and (b) the ratio of reflection coefficient.
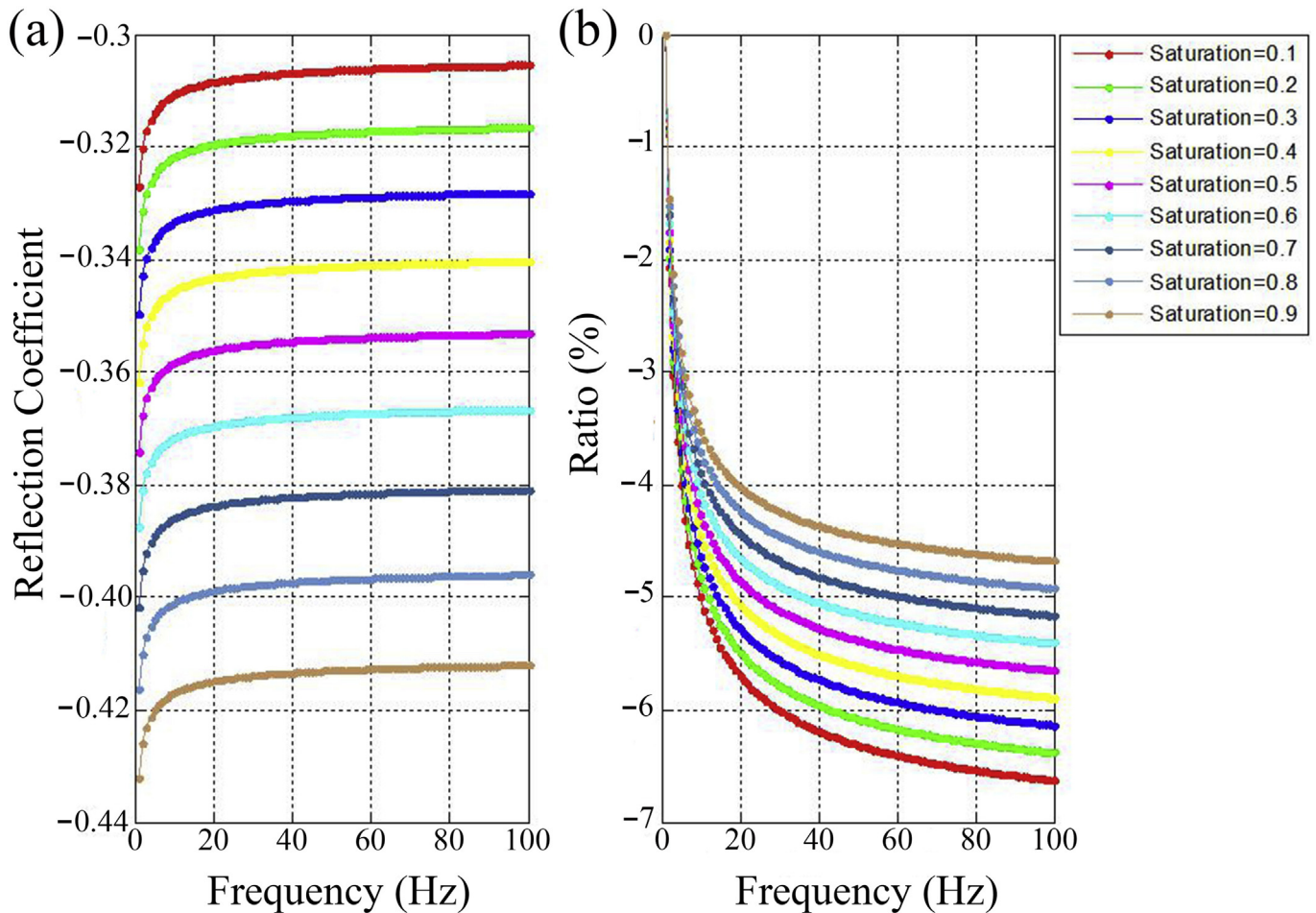
Figure 2. (a) The absolute change of reflection coefficient versus frequency with different saturation of gas hydrate and (b) the ratio of reflection coefficient.

is $S_h = 0.1$. In the lower layer, the porosity is $\phi_2 = 0.55$, the permeability is $k_2 = 10$ mD. Then we can calculate the RVF curves.

When gas exists beneath the fracture-filling gas hydrate sediment, the reflection coefficient at BSR is negative (Fig. 3). With the increase of frequency, the absolute value of reflection coefficient increases. That is to say, the energy of the high frequency reflected wave is strong and the energy of the low frequency reflected wave is weak. The reflection coefficient variance with frequency is prominent at small incident angle.

From Fig. 4 we can see, with the increasing saturation of gas hydrate, the absolute value of reflection coefficient decreases. The reflection coefficient variance with frequency is prominent at small saturation of gas hydrate.

5. Application

5.1. The calculation method of reflection coefficient versus frequency curve

For one trace of seismic data, seismic record $x(t)$ equals the convolution of the reflection coefficient $r(t)$ and wavelet $w(t)$.

$$x(t) = r(t)*w(t) \tag{19}$$

After the Fourier transform, we can get the expression in frequency domain.

$$X(f) = R(f)W(f) \tag{20}$$

where $X(f)$, $R(f)$ and $W(f)$ are respectively frequency responses of the seismic record, the reflection coefficient and the wavelet. We can get the expression of reflection coefficient in frequency domain.

$$R(f) = X(f)/W(f) \tag{21}$$

In order to get the reflection coefficient versus frequency curve, we conduct the ST transform on the data and get the frequency response $X(f)$ of every sample. We then calculate the spectrum of the whole trace data $w(t)$. Through the process of spectrum simulation and calculating the spectrum's envelope, the interference can be eliminated and the frequency response of wavelet $W(f)$ can be derived. The reflection coefficient versus frequency curve can then be obtained.

5.2. Numerical examples

This study area is located in the northeastern continental slope of South China Sea (SCS). The two sites 08 and 16 are used in this study (Fig. 5). Bottom Simulating Reflection (BSR) and blanking zones indicating the existence of gas hydrate in SCS were reported by some researchers (Song and Geng, 2000; Wu et al., 2005).

Gas hydrate-bearing sediments identified from the coring include two main morphologies; invisible pore-filling gas hydrates and visible fracture filling, nodules, and massive gas hydrates. Disseminated, or called pore-filling, gas hydrate in deep fine-grained sediments was identified in site 16. Fracture filling gas hydrate was found in fine-grained sediments at sites 08 and 16.
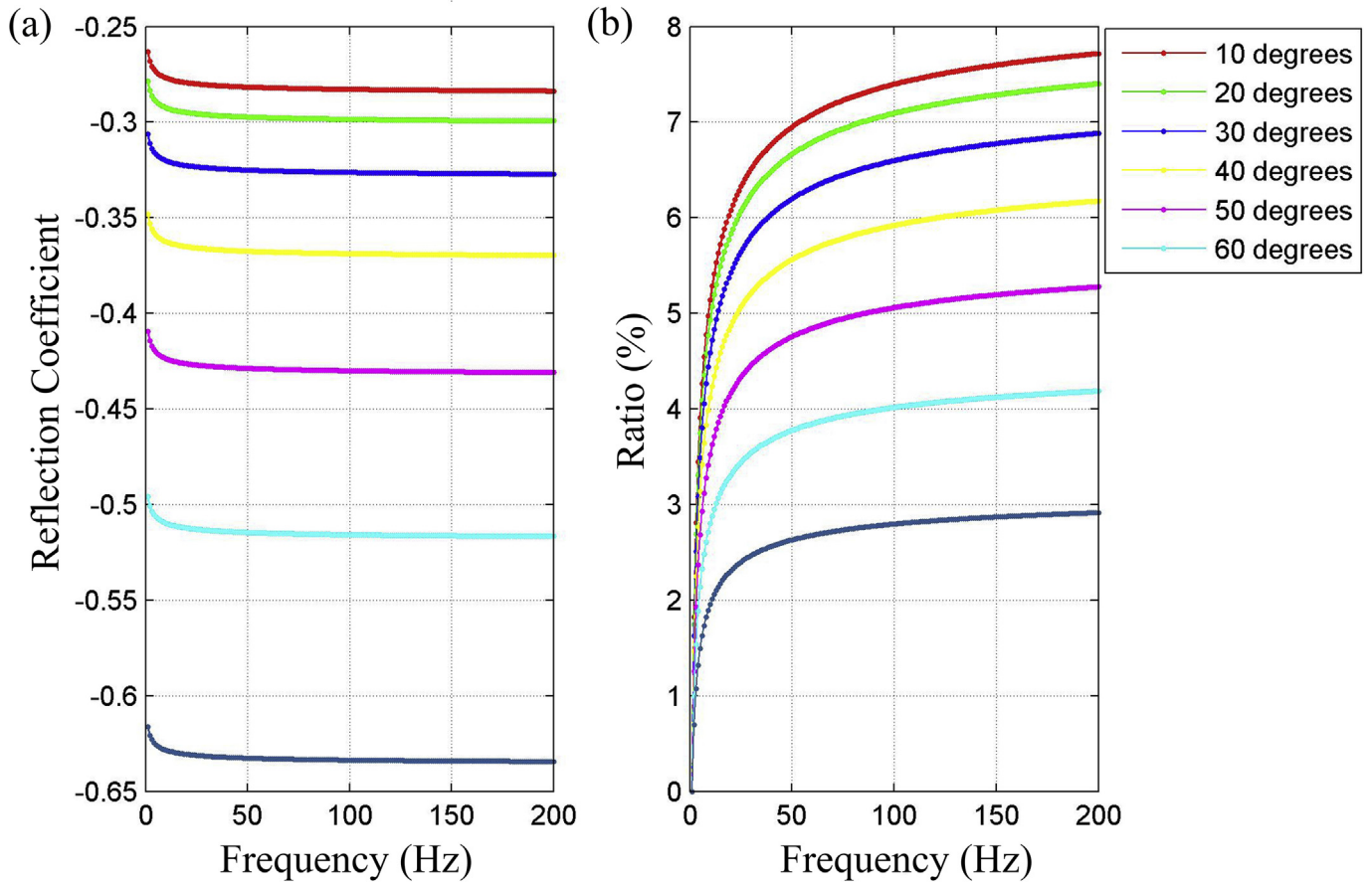
Figure 3. (a) The absolute change of reflection coefficient versus frequency with different incident angles and (b) the ratio of reflection coefficient.
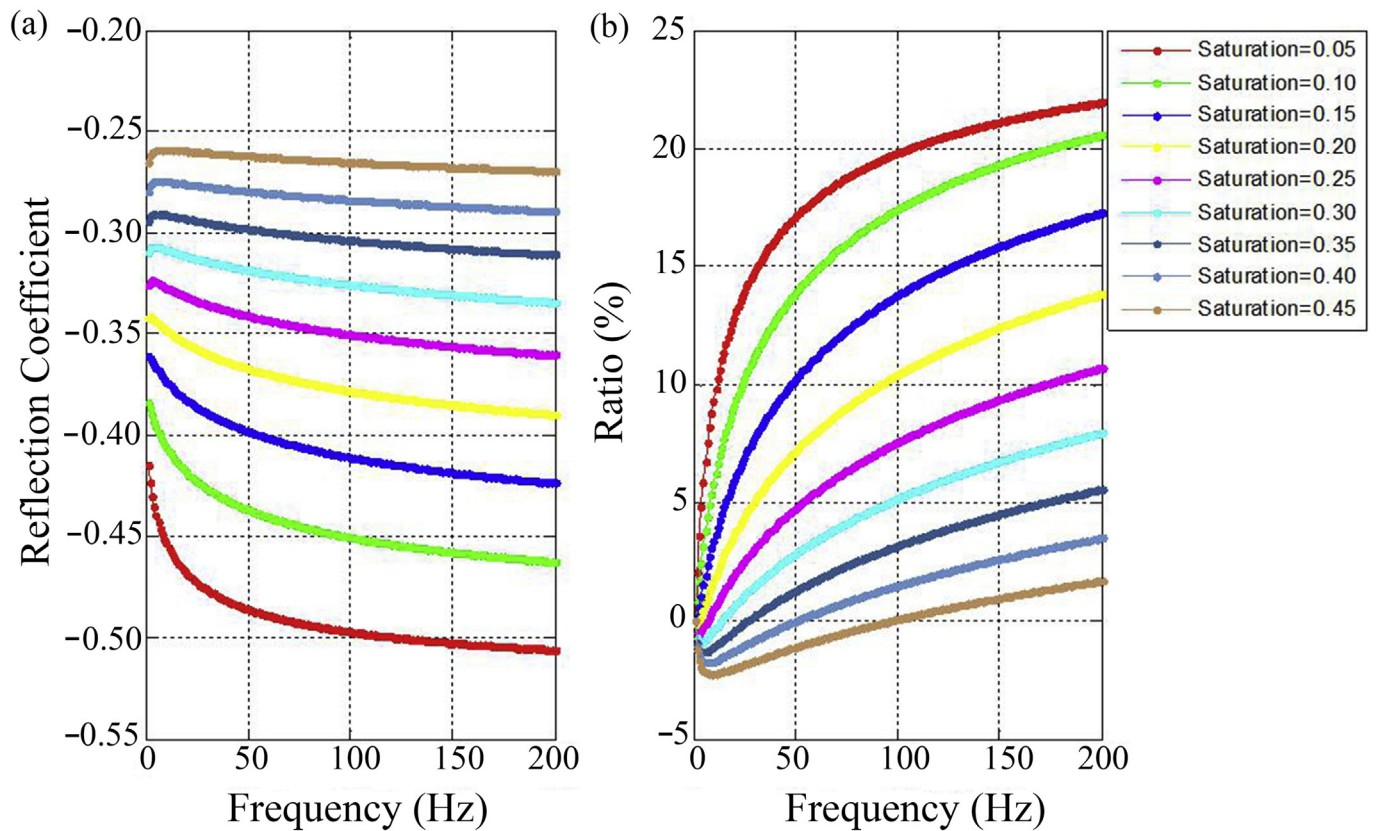

Figure 4. (a) The absolute change of reflection coefficient versus frequency with different saturation of gas hydrate and (b) the ratio of reflection coefficient.
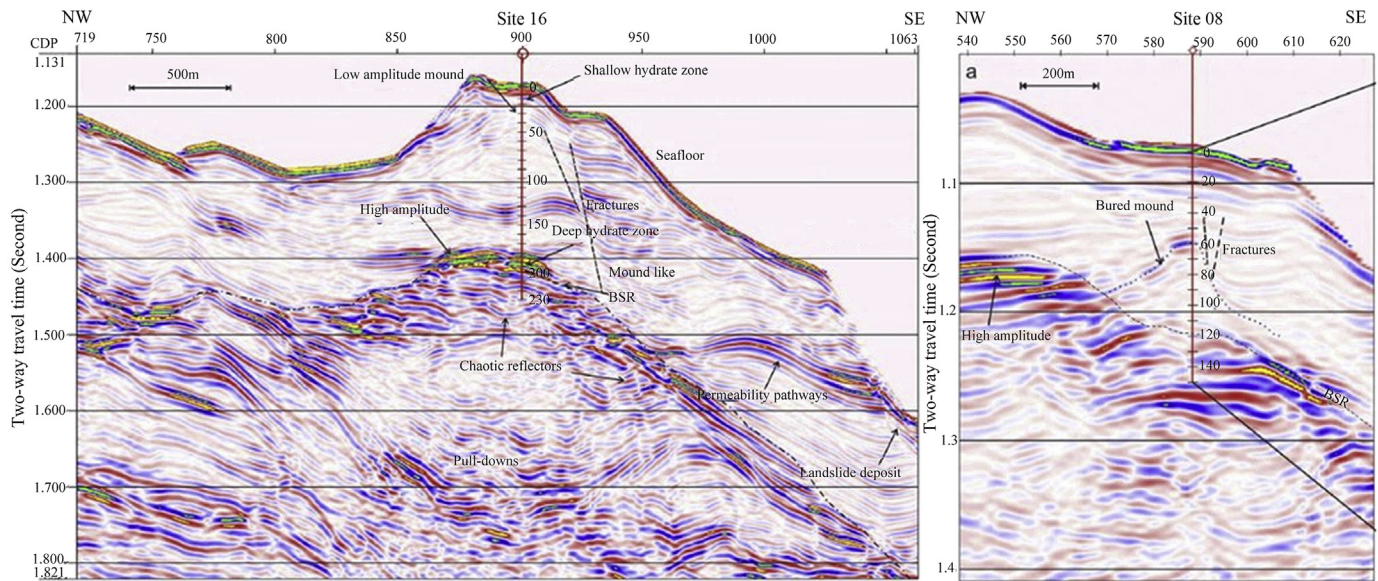
Figure 5. Seismic section through sites 16 and 08 (Sha et al., 2015).

5.2.1. Site 16

The drilling results have shown that there exists both the pore-filling gas hydrate and the fracture-filling gas hydrate at site 16. The fracture-filling gas hydrate zone locates at 1.18 s in the shallow area in the section. The pore-filling gas hydrate zone locates at 1.42 s in the deep area (Sha et al., 2015). We calculate the reflection coefficient dispersion at this area and identify the gas hydrate morphology based on the forward modeling conclusions.

From Fig. 6 we can see the energy of high frequency reflected waves is stronger than low frequency at shallow BSR while the energy of low frequency reflected waves is stronger at deep BSR. One point should be illustrated, that the concept of BSR at shallow area indicates the bottom of gas hydrate zone. In fact the double BSR doesn't exist at this area, we just use a unified concept of BSR in

order for convenience of discussion. According to our theory, if the sediments contain pore-filling gas hydrate, the energy of low frequency reflected wave will be strong and if the sediments contain fracture-filling gas hydrate, the energy of high frequency reflected wave will be strong. That is to say, if there exists gas hydrate near two BSR, we can identify that the shallow sediments contain fracture-filling gas hydrate and the deep position contains pore-filling gas hydrate. In fact, the drilling at site 16 shows that the near-surface gas hydrate is fracture-filling and the pore-filling gas hydrate exists at deep position.

5.2.2. Site 08

The drilling results have shown that there exists fracture-filling gas hydrate at site 08. The fracture-filling gas hydrate zone locates
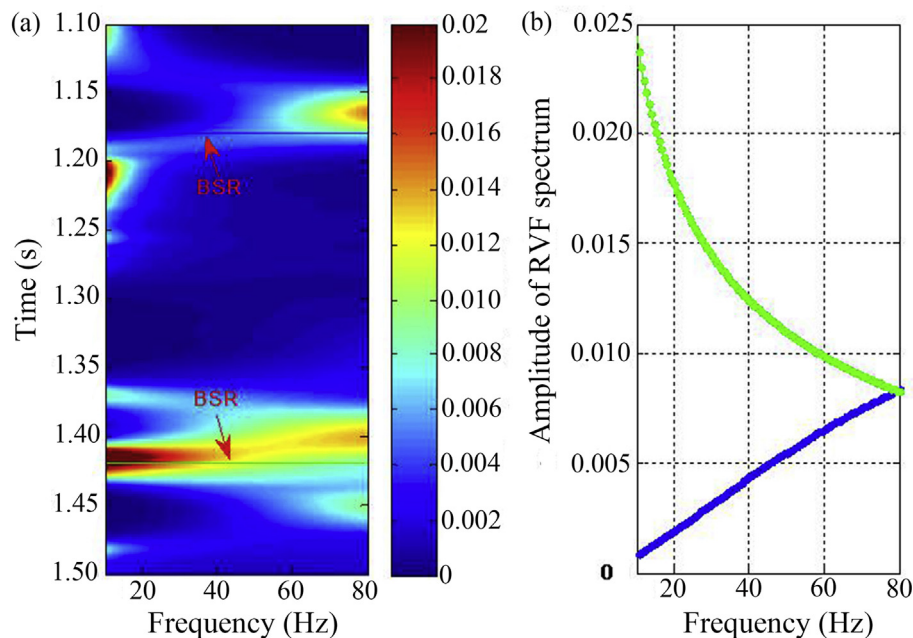

Figure 6. The RVF analysis near site 16. (a) The frequency spectrum of reflection coefficient and (b) the RVF curve at BSR. The green and blue lines in (a) represent BSR and we can get the corresponding RVF curve with the same color in (b).

Figure 7. The RVF analysis near site 08. (a) The frequency spectrum of reflection coefficient and (b) the RVF curve at BSR. The green and blue lines in (a) represent BSR and we can get the corresponding RVF curve with the same color in (b).
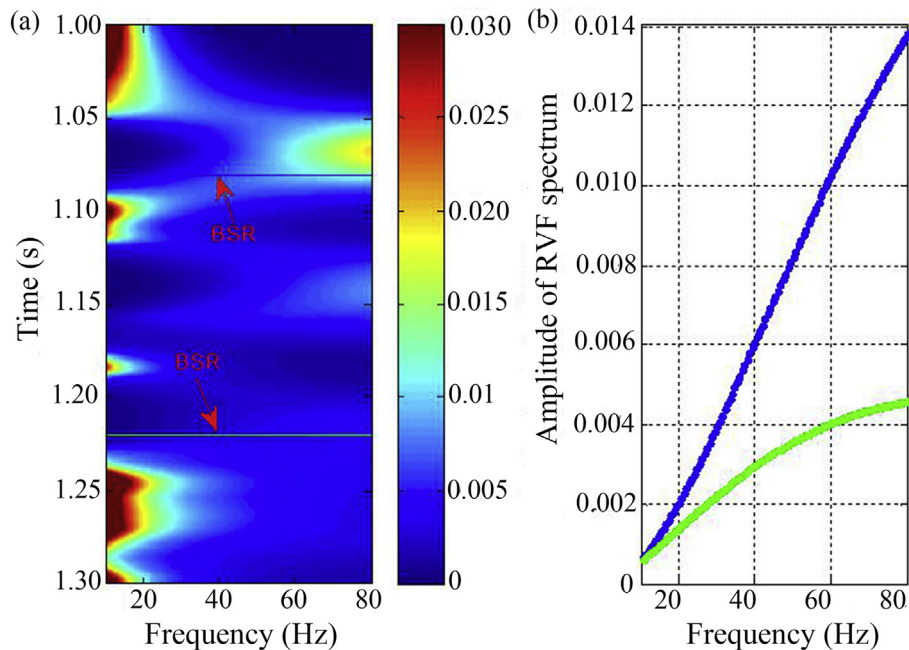
at 1.08 s and 1.22 s in the section (Fig. 5). We will calculate the reflection coefficient dispersion at these areas and identify the gas hydrate morphology.

From Fig. 7 we can see the energy of the high frequency reflected wave is stronger than low frequency wave at two BSR. The concept of BSR at shallow area also means the bottom of gas hydrate zone. We can identify that the two positions contain fracture-filling gas hydrate. Indeed, the drilling at site 08 shows the existence of the fracture-filling gas hydrate.

6. Discussion

Seismic waves propagating in heterogeneous porous media create fluid pressure gradients and consequently induce fluid flow. The wave-induced fluid flow typically affects wave propagation characteristics, and hence it affects the behavior of reflection coefficients. The most pronounced influence is that the reflection coefficients are frequency dependent. The mesoscopic-loss mechanism can be used to describe the wave's energy loss at seismic frequency band (10^0–10^2 Hz) (Pride et al., 2004).

In this paper, we use the mesoscopic-loss theory to study the frequency dependent reflection at BSR of the gas hydrate contained layer. We assume the BSR to be the interface between the upper gas hydrate sediments and the lower gas contained layer. In reality, we know not all BSR can meet this assumption, but, it represents a typical case where the BSR exists.

When seismic waves pass through the pore-filling gas hydrate sediments, the high frequency energy is reduced, while the low frequency energy of reflected waves at BSR is strong. When seismic waves pass through the fracture-filling gas hydrate sediments, the high frequency wave is propagated and its reflected energy at BSR is strong. We utilize this difference to identify the gas hydrate morphology in northern South China Sea and the conclusions are corresponding well with the drilling results.

There still exists some problems that need to discuss in the future research. White's model is useful to patchy gas saturation. However, for gas hydrate in the pore space, it is different from gas.

The error caused by the differences should be considered. In the forward modeling part, the effect on results from the physical parameters such as porosity, permeability, rock matrix, the structure of pore space should be discussed in future work. In application, the key is to find the bottom of gas hydrate sediments. The BSR usually indicates the bottom position, so clear BSR could improve the effectiveness in identifying the gas hydrate morphology.

7. Conclusion

Gas hydrate-bearing sediments include two main morphologies. They are pore-filling gas hydrates and fracture-filling gas hydrates. We use the mesoscopic-loss mechanism to do the forward modeling to study the reflection coefficient versus frequency at BSR of the gas hydrate layer. When gas exists beneath the fracture-filling gas hydrate sediment, the energy of the low frequency reflected wave is strong and the energy of the high frequency reflected wave is weak at BSR. As for the fracture-filling gas hydrate, the energy of high frequency reflected wave is stronger at BSR. This difference can be used to identify the gas hydrate morphology. We use this method to predict the gas hydrate types in northern South China Sea and get the same results with the site drilling.

Appendix

In double porosity theory, the mesoscopic heterogeneity is modeled as a mixture of two porous phases saturated by a single fluid. This theory can be described by the governing equations and

the fluid transport equations. The governing equations dominate the wave's propagation through the pores. The fluid transport equations describe the attenuation by controlling the fluid transport.

1. Local governing equations

Each porous phases is locally modeled as a porous continuum and obeys the laws of poroelasticity (e.g., Biot, 1962)

$$\nabla \cdot \tau_i^D - \nabla p_{ci} = \rho \ddot{u}_i + \rho_f \dot{Q}_i \qquad \text{A-1}$$

$$Q_i = -\frac{k_i}{\eta}\left(\nabla p_{fi} + \rho_f \ddot{u}_i\right) \qquad \text{A-2}$$

$$\begin{bmatrix} \nabla \cdot \dot{u}_i \\ \nabla \cdot Q_i \end{bmatrix} = -\frac{1}{K_i^d}\begin{bmatrix} 1 & -\alpha_i \\ -\alpha_i & \alpha_i/B_i \end{bmatrix}\begin{bmatrix} \dot{p}_{ci} \\ \dot{p}_{fi} \end{bmatrix} \qquad \text{A-3}$$

$$\tau_i^D = G_i\left(\nabla u_i + \nabla u_i^T - \frac{2}{3}\nabla \cdot u_i I\right) \qquad \text{A-4}$$

where the index i represents the two phases ($i = 1, 2$). The response fields in these equations are themselves local volume averages taken over a scale larger than the grain sizes but smaller than the mesoscopic extent of either phase. The local fields are: u_i, the average displacement of the framework of grains; Q_i, the Darcy filtration velocity; p_{fi}, the fluid pressure; p_{ci}, the confining pressure (total average pressure); and τ_i, the deviatoric (or shear) stress tensor. In the linear theory of interest here, the overdots on these fields denote a partial time derivative. In the local Darcy law (A-2), η is the fluid viscosity and k_i is the permeability.

In the local compressibility law (A-3), K_i^d is the drained bulk modulus of phase i (confining pressure change divided by sample dilatation under conditions where the fluid pressure does not change), B_i is Skempton (1954) coefficient of phase i (fluid pressure change divided by confining pressure change for a sealed sample), and α_i is the Biot and Willis (1957) coefficient of phase i defined as

$$\alpha_i = \left(1 - K_i^d / K_i^u\right)/B_i \qquad \text{A-5}$$

where K_i^u is the undrained bulk modulus (confining pressure change divided by sample dilatation for a sealed sample). In the present work, no restrictions to single-mineral isotropic grains will be made. Finally, in the deviatoric constitutive law (A-4), G_i is the shear modulus of the framework of grains. At the local level, all these poroelastic constants are taken to be real constants. The Gassmann (1951) fluid substitution relations allow B_i and α_i to be expressed in terms of the porosity ϕ_i, the fluid and solid bulk moduli K_f and K_S, and the drained modulus K_i^d.

2. Double-porosity governing equations

In the double-porosity theory, the goal is to determine the average fluid response in each of the porous phases in addition to the average displacement of the solid grains (Berryman and Wang, 1995). The averages are taken over regions large enough to significantly represent both porous phases, but smaller than wavelengths. Assuming an $e^{-i\omega t}$ time dependence, Pride and Berryman (2003a) have volume averaged the local laws (A-1)–(A-4) to obtain the macroscopic "double-porosity" governing equations in the form

$$\nabla \cdot \tau^D - \nabla P_c = -i\omega\left(\rho v + \rho_f q_1 + \rho_f q_2\right) \qquad \text{A-6}$$

$$\begin{bmatrix} q_1 \\ q_2 \end{bmatrix} = -\frac{1}{\eta}\begin{bmatrix} \kappa_{11} & \kappa_{12} \\ \kappa_{12} & \kappa_{22} \end{bmatrix} \cdot \begin{bmatrix} \nabla \bar{p}_{f1} - i\omega\rho_f v \\ \nabla \bar{p}_{f2} - i\omega\rho_f v \end{bmatrix} \qquad \text{A-7}$$

$$\begin{bmatrix} \nabla \cdot v \\ \nabla \cdot q_1 \\ \nabla \cdot q_2 \end{bmatrix} = i\omega\begin{bmatrix} a_{11} & a_{12} & a_{13} \\ a_{12} & a_{22} & a_{23} \\ a_{13} & a_{23} & a_{33} \end{bmatrix} \cdot \begin{bmatrix} P_c \\ \bar{p}_{f1} \\ \bar{p}_{f2} \end{bmatrix} + i\omega\begin{bmatrix} 0 \\ \zeta_{int} \\ -\zeta_{int} \end{bmatrix} \qquad \text{A-8}$$

$$-i\omega\zeta_{int} = \gamma(\omega)\left(\bar{p}_{f1} - \bar{p}_{f2}\right) \qquad \text{A-9}$$

$$-i\omega\tau^D = [G(\omega) - i\omega g(\omega)]\left[\nabla v + (\nabla v)^T - \frac{2}{3}\nabla \cdot v I\right] \qquad \text{A-10}$$

The macroscopic fields are v, the average particle velocity of the solid grains throughout an averaging volume of the composite; q_i, the average Darcy flux across phase i; P_c, the average total pressure in the averaging volume; τ^D, the average deviatoric stress tensor; $\bar{p}_{fi}$, the average fluid pressure within phase i; and $-i\omega\zeta_{int}$, the average rate at which fluid volume is being transferred from phase 1 into phase 2 as normalized by the total volume of the averaging region. The dimensionless increment ζ_{int} represents the "mesoscopic flow."

Eq. (A-7) is the generalized Darcy law allowing for fluid cross coupling between the phases (Pride and Berryman, 2003b), Eq. (A-8) is the generalized compressibility law where $\nabla \cdot q_i$ corresponds to fluid that has been depleted from phase i due to transfer across the external surface of an averaging volume, and Eq. (A-9) is the transport law for internal mesoscopic flow (fluid transfer between the two porous phases).

3. Reduction to an effective Biot theory

The approach that we take instead is to first reduce these double-porosity laws (A-6)–(A-10) to an effective single-porosity Biot theory having complex frequency-dependent coefficients. The easiest way to do this is to assume that phase 2 is entirely embedded in phase 1 so that the average flux q_2 into and out of the averaging volume across the external surface of phase 2 is zero. By placing $\nabla \cdot q_2 = 0$ into the compressibility laws A-8, the fluid pressure $\bar{p}_{f2}$ can be entirely eliminated from the theory. In this case the double-porosity laws reduce to effective single-porosity poroelasticity governed by laws of the form A-3 but with effective poroelastic moduli given by

$$\frac{1}{K_D} = a_{11} - \frac{a_{13}^2}{a_{33} - \gamma/i\omega} \qquad \text{A-11}$$

$$B = \frac{-a_{12}(a_{33} - \gamma/i\omega) + a_{13}(a_{23} + \gamma/i\omega)}{(a_{22} - \gamma/i\omega)(a_{33} - \gamma/i\omega) - (a_{23} + \gamma/i\omega)^2} \qquad \text{A-12}$$

$$\frac{1}{K_U} = \frac{1}{K_D} + B\left(a_{12} - \frac{a_{13}(a_{23} + \gamma/i\omega)}{a_{33} - \gamma/i\omega}\right) \qquad \text{A-13}$$

here, $K_D(\omega)$ is the effective drained bulk modulus of the double-porosity composite, $B(\omega)$ is the effective Skempton's coefficient, and $K_U(\omega)$ is the effective undrained bulk modulus. An effective Biot-Willis constant can then be defined using $\alpha(\omega) = [1 - K_D(\omega)/K_U(\omega)]/B(\omega)$.

4. Double-porosity a_{ij} coefficients

The constants a_{ij} are all real and correspond to the high-frequency response for which no internal fluid pressure relaxation can take place. They are given exactly as (Pride and Berryman, 2003a):

$$a_{11} = 1/K \qquad \text{A-14}$$

$$a_{22} = \frac{v_1 \alpha_1}{K_1^d} \left(\frac{1}{B_1} - \frac{\alpha_1(1-Q_1)}{1 - K_1^d / K_2^d} \right) \qquad \text{A-15}$$

$$a_{33} = \frac{v_2 \alpha_2}{K_2^d} \left(\frac{1}{B_2} - \frac{\alpha_2(1-Q_2)}{1 - K_2^d / K_1^d} \right) \qquad \text{A-16}$$

$$a_{12} = -v_1 Q_1 \alpha_1 / K_1^d \qquad \text{A-17}$$

$$a_{13} = -v_2 Q_2 \alpha_2 / K_2^d \qquad \text{A-18}$$

$$a_{23} = -\frac{\alpha_1 \alpha_2 K_1^d / K_2^d}{\left(1 - K_1^d / K_2^d \right)} \left(\frac{1}{K} - \frac{v_1}{K_1^d} - \frac{v_2}{K_2^d} \right) \qquad \text{A-19}$$

where Q_i is the auxiliary constant given by

$$v_1 Q_1 = \frac{1 - K_2^d / K}{1 - K_2^d / K_1^d}, \quad v_2 Q_2 = \frac{1 - K_1^d / K}{1 - K_1^d / K_2^d} \qquad \text{A-20}$$

here, v_1 and v_2 are the volume fractions of each phase within an averaging volume of the composite. In the paper, $v_2 = S_h$, $v_1 = 1 - S_h$, S_h is the saturation of gas hydrates.

The one constant in these a_{ij} that has not yet been determined is the overall drained modulus $K = 1/a_{11}$ of the two-phase composite (the modulus defined in the quasi-static limit where the local fluid pressure throughout the composite is everywhere unchanged).

The Hashin and Shtrikman (1963) bounded for the overall low-frequency drained bulk modulus K and shear modulus G of the composite can be written

$$\frac{1}{K + 4G_i/3} = \frac{v_1}{K_1^d + 4G_i/3} + \frac{v_2}{K_2^d + 4G_i/3} \qquad \text{A-21}$$

$$\frac{1}{G + \varsigma_i} = \frac{v_1}{G_1 + \varsigma_i} + \frac{v_2}{G_2 + \varsigma_i} \qquad \text{A-22}$$

where ς_i is defined

$$\varsigma_i = \frac{G_i \left(9K_i^d + 8G_i \right)}{6 \left(K_i^d + 2G_i \right)} \qquad \text{A-23}$$

We will find it natural to define phase 2 as being more compliant than phase 1 so that $K_2^d < K_1^d$ and $G_2 < G_1$. In this case, the upper limits for K and G are obtained by taking $i = 1$ and the lower limits by taking $i = 2$. In each of these cases, the lower Hashin and Shtrikman (1963) bounds are more appropriate than the upper bounds. Our modeling suggestion is simply to use the lower bounds for modeling K and G in these situations.

In order to use the unified double-porosity framework of the present paper, it is convenient to have models for the various porous continuum constituent properties.

For consolidated part (phase 1) of the continuum, the moduli are

$$K_1^d = K_1^s \frac{1 - \phi_1}{1 + c\phi_1} \qquad \text{A-24}$$

$$G_1 = G_1^s \frac{1 - \phi_1}{1 + 3c\phi_1/2} \qquad \text{A-25}$$

The consolidation parameter c represents the degree of consolidation between the grains, c = 10. The K_1^s and G_1^s are the mineral moduli of the grains. The minerals of phase 1 consist of 60% clay +35% calcite +5% quartz, $K_1^s = 35$ GPa, $G_1^s = 13.8$ GPa, the density $\rho_1^s = 2.63$ g/cm^3.

5. Double-porosity transport

Normally, the double-porosity model is useful (or necessary) only in situations where the two phases have strong contrasts in their physical properties. When the embedded phase 2 is much more permeable than the host phase 1, Pride and Berryman (2003b) obtained

$$\gamma_m = -\frac{k_1 K_1^d}{\eta L^2} \left(\frac{a_{12} + B_0(a_{22} + a_{33})}{R_1 - B_0/B_1} \right) \qquad \text{A-26}$$

where a_{ij} is given by Eqs. (A-14)–(A-19) and the remaining terms B_o, L and R_1 are now defined.

The dimensionless quantity B_o is the static Skempton's coefficient for the composite and is given exactly by

$$B_0 = -\frac{a_{12} + a_{13}}{a_{22} + 2a_{23} + a_{33}} \qquad \text{A-27}$$

regardless of the mesoscopic geometry.

The length $L^2 = a^2/15$, which characterizes the average distance in phases. a is the radius of each sphere of phase 2.

The dimensionless quantity R_1 is the ratio of the average static confining pressure in phase 1 to the pressure applied to the external surface of a sealed sample of the composite. Pride and Berryman (2003a) derived this ratio to be

$$R_1 = Q_1 + \frac{\alpha_1(1-Q_1)B_0}{1 - K_1^d / K_2^d} - \frac{v_2}{v_1} \frac{\alpha_2(1-Q_2)B_0}{1 - K_2^d / K_1^d} \qquad \text{A-28}$$

The transition frequency ω_m corresponds to the onset of a high-frequency regime in which the fluid pressure diffusion penetration distance between the phases becomes small relative to the scale of the mesoscopic heterogeneity. It is given by Pride and Berryman (2003b) to be

$$\omega_m = \frac{\eta B_1 K_1^d}{k_1 \alpha_1} \left(\gamma_m \frac{V}{S} \right)^2 \left(1 + \sqrt{\frac{k_1 B_2 K_2^d \alpha_1}{k_2 B_1 K_1^d \alpha_2}} \right)^2 \qquad \text{A-29}$$

The length V/S is the volume-to-surface ratio. The model has the following geometric properties: $a = 1$cm, $V/S = 5$ mm.

For unconsolidated part (phase 2) of the continuum, the moduli are

$$K_2^d = \frac{1}{6} \left[\frac{4(1-\phi_0)^2 n_o^2 P_0}{\pi^4 C_S^2} \right]^{1/3} \frac{(P_e/P_0)^{1/2}}{\left\{ 1 + [16P_e/(9P_0)]^4 \right\}^{1/24}} \qquad \text{A-30}$$

$$G_2 = 3K_2^d / 5 \qquad \text{A-31}$$

where P_e is the effective overburden pressure, $P_e = (1 - \phi_2)(\rho_2^s - \rho_f)gh$, g is the gravity and h is overburden thickness, $g = 9.81\ m/s^2$. The BSR is evident on seismic data from the area at a depth of 200 mbsf. This depth is inferred from logs to be the maximum depth of hydrate occurrence. So we let $h = 200$ m. The porosity of the grain pack is ϕ_0 and the compliance parameter C_s is defined.

$$C_S = \frac{1}{4\pi}\left(\frac{1}{G_2^s} + \frac{1}{K_2^s + G_2^s/3}\right) \qquad\qquad \text{A-32}$$

where K_2^s and G_2^s are the moduli of solid gas hydrate. $\phi_0 = 0.6$, $n_0 = 9$, $P_0 = 10$ MPa.

References

Berryman, J.G., Wang, H.F., 1995. The elastic coefficients of double-porosity models for fluid transport in jointed rock. Journal of Geophysical Research Solid Earth 100, 24611–24627.

Biot, M.A., 1962. Mechanics of deformation and acoustic propagation in porous media. Journal of Applied Physics 33, 1482–1498.

Biot, M.A., Willis, D.G., 1957. The elastic coefficients of the theory of consolidation. Journal of Applied Mechanics 15, 594–601.

Carcione, J.M., Picotti, S., 2006. P-wave seismic attenuation by slow-wave diffusion: effects of inhomogeneous rock properties. Geophysics 71 (3), O1–O8.

Gassmann, F., 1951. Über die Elastizität poröser Medien. Vierteljahrsschrift der Naturforschenden Gesellschaft Zuerich 96, 1–23.

Hashin, Z., Shtrikman, S., 1963. A variational approach to the theory of the elastic behavior of multiphase materials. Journal of the Mechanics and Physics of Solids 11, 127–140.

Li, C.H., Zhao, Q., Xu, H.J., 2014. Relation between relative permeability and hydrate saturation in Shenhu area, South China Sea. Applied Geophysics 11 (2), 207–214.

Pride, S.R., Berryman, J.R., 2003a. Linear dynamics of double-porosity and dual-permeability materials. Governing equations and acoustic attenuation. Physical Review E Statistical Nonlinear and Soft Matter Physics 68, 036603.

Pride, S.R., Berryman, J.G., 2003b. Linear dynamics of double-porosity and dual-permeability materials. Fluid transport equations. Physical Review E Statistical Nonlinear and Soft Matter Physics 68, 036604.

Pride, S.R., Berryman, J.G., Harris, J.M., 2004. Seismic attenuation due to wave-induced flow. Journal of Geophysical Research 109, B01201. https://doi.org/10.1029/2003JB002639.

Sha, Z.B., Liang, J.Q., Zhang, G.X., Yang, S.X., Lu, J.G., Zhang, Z.J., McConnel, D.R., Humphrey, G., 2015. A seepage gas hydrate system in northern South China Sea: seismic and well log interpretations. Marine Geology 366, 69–78.

Skempton, A.W., 1954. The pore-pressure coefficients A and B. Geotechnique 4, 143–147.

Song, H.B., Geng, J.H., 2000. Geophysical evidence of gas hydrates existence in Dongsha region north of South China Sea. EOS Transactions on AGU 81 (48), 635.

Wang, X.J., Wu, S.G., Liu, X.W., Sun, Y.B., Yang, S.X., 2009. Characteristic analysis and saturation estimation of gas hydrate in Dongsha area. Geophysical Prospecting for Petroleum 48 (5), 445–452.

White, J.E., Mikhaylova, N.G., Lyakhovitskiy, F.M., 1975. Low-frequency seismic waves in fluid saturated layered rocks: Izvestija Academy of Sciences USSR. Physics of the Solid Earth 11, 654–659.

Wu, S.G., Zhang, G.X., Huang, Y.Y., Liang, J.Q., Wong, H.K., 2005. Gas hydrate occurrence on the northern slope of the South China Sea. Marine and Petroleum Geology 22, 403–412.

Yang, S., Zhang, G., Zhang, M., Liang, J., Lu, J., Schultheiss, P., Holland, M., 2014. A complex gas hydrate system in the Dongsha area, South China Sea: results from drilling expedition GMGS2. In: Proceedings of the 8th International Conference on Gas Hydrates (ICGH8–2014), Beijing, China, 28 July-1 August, 2014.

Zhang, H., Yang, S., Wu, N., Schultheiss, P., GMGS-1 Science Team, 2007. China's first gas hydrate expedition successful: fire in the Ice. Methane Hydrate Newsletter 7 (2), 4–8.

Zhang, Z., Mcconnell, D., Yao, Q., 2014a. Velocities and attenuations of gas hydrate-bearing sediments in fractured and sand reservoirs. In: Proceedings of the Eighth International Conference on Gas Hydrates, July 28-August 1, 2014, Beijing, China.

Zhang, G., Yang, S., Zhang, M., Liang, J., Lu, J., Melanie, H., Peter, S., GMGS2 Science Team, 2014b. Gmgs2 investigates a rich and complex gas hydrate environment in the South China Sea: fire in the ice. Methane Hydrate Newsletter 14 (1), 1–5.